Acta Oceanol. Sin., 2021, Vol. 40, No. 11, P. 176–188
https://doi.org/10.1007/s13131-021-1839-6
http://www.aosocean.com
E-mail: ocean2@hyxb.org.cn

Arctic sea ice concentration retrieval using the DT-ASI algorithm based on FY-3B/MWRI data

Hairui Hao[1, 2], Jie Su[1, 2, 3]*, Qian Shi[1, 4], Lele Li[5]

[1] Key Laboratory of Physical Oceanography of Ministry of Education, Ocean University of China, Qingdao 266100, China

[2] University Corporation for Polar Research, Beijing 100875, China

[3] Pilot National Laboratory for Marine Science and Technology (Qingdao), Qingdao 266237, China

[4] Southern Marine Science and Engineering Guangdong Laboratory (Zhuhai), Zhuhai 519082, China

[5] Faculty of Information Science and Engineering, Ocean University of China, Qingdao 266100, China

Received 19 May 2020; accepted 2 April 2021

Abstract

Sea ice concentration (SIC) is one of the most important indicators when monitoring climate changes in the polar region. With the development of the Chinese satellite technology, the FengYun (FY) series has been applied to retrieve the sea ice parameters in the polar region. In this paper, to improve the SIC retrieval accuracy from the passive microwave (PM) data of the Microwave Radiation Imager (MWRI) aboard on the FengYun-3B (FY-3B) Satellite, the dynamic tie-point (DT) Arctic Radiation and Turbulence Interaction Study (ARTIST) Sea Ice (ASI) (DT-ASI) SIC retrieval algorithm is applied and obtained Arctic SIC data for nearly 10 a (from November 18, 2010 to August 19, 2019). Also, by applying a land spillover correction scheme, the erroneous sea ice along coastlines in melt season is removed. The results of FY-3B/DT-ASI are obviously improved compared to that of FY-3B/NT2 (NASA-Team2) in both SIC and sea ice extent (SIE), and are highly consistent with the results of similar products of AMSR2 (Advanced Microwave Scanning Radiometer 2)/ASI and AMSR2/DT-ASI. Compared with the annual average SIC of FY-3B/NT2, our result is reduced by 2.31%. The annual average SIE difference between the two FY-3Bs is 1.65×10^6 km^2, of which the DT-ASI algorithm contributes 87.9% and the land spillover method contributes 12.1%. We further select 58 MODIS (Moderate-resolution Imaging Spectroradiometer) cloud-free samples in the Arctic region and use the tie-point method to retrieve SIC to verify the accuracy of these SIC products. The root mean square difference (RMSD) and mean absolute difference (MAD) of the FY-3B/DT-ASI and MODIS results are 17.2% and 12.7%, which is close to those of two AMSR2 products with 6.25 km resolution and decreased 8% and 7.2% compared with FY-3B/NT2. Further, FY-3B/DT-ASI has the most significant improvement where the SIC is lower than 60%. A high-quality SIC product can be obtained by using the DT-ASI algorithm and our work will be beneficial to promote the application of FengYun Satellite.

Key words: DT-ASI, FY-3B/MWRI, sea ice concentration, MODIS

Citation: Hao Hairui, Su Jie, Shi Qian, Li Lele. 2021. Arctic sea ice concentration retrieval using the DT-ASI algorithm based on FY-3B/MWRI data. Acta Oceanologica Sinica, 40(11): 176–188, doi: 10.1007/s13131-021-1839-6

1 Introduction

The high albedo of sea ice can effectively hinder the exchange of heat between the atmosphere and the ocean (Comiso et al., 2003; Hall et al., 2004). With global warming in recent decades, Arctic sea ice has become one of the most obvious indications of global climate change (Comiso et al., 2017). Continuous observations by satellites have shown that Arctic sea ice has undergone tremendous decadal changes (Bjørgo et al., 1997; Cavalieri et al., 1997). These changes affect the absorption of solar radiation in the Arctic during summertime and have a positive feedback effect on global warming (Perovich et al., 2007). Arctic sea ice even has a role in regulating the climate of the Northern Hemisphere (Cvijanovic et al., 2015). The rapid melting of Arctic sea ice and the extension of the melting season provide favorable conditions for the opening of Arctic waterways (Li et al., 2016).

Sea ice concentration (SIC), defined as the proportion of area covered by sea ice to the total footprint area, is an essential parameter to measure Arctic sea ice distribution. Sea ice extent (SIE) and sea ice area (SIA) can be further obtained from SIC data. With the development of remote sensing technology, more and more satellite sensors, including visible light and near-infrared radiometers, imaging spectrometers, and active and passive microwave (PM) radiometers, are now being used for SIC estimates (Cao and Jin, 2006). Among them, SIC derived from PM remote sensing data has a better temporal and spatial continuity.

Currently, many SIC retrieval algorithms based on PM data are in use. The NASA Team (NT) algorithm (Cavalieri et al., 1984), the Bootstrap algorithm (Comiso, 1995) and the Bristol algorithm (Smith, 1996) all use low-resolution brightness temperature (BT) at 19 GHz and 37 GHz from the Scanning Multichan-

Foundation item: The National Key Research and Development Program of China under contract No. 2016YFC1402704; the National Natural Science Foundation of China under contract Nos 41941012 and 42076228; the Guangdong Basic and Applied Basic Research Foundation under contract No. 2019A1515110295.

*Corresponding author, E-mail: sujie@ouc.edu.cn

nel Microwave Radiometer (SMMR), the Special Sensor Microwave Imager (SSM/I), the Special Sensor Microwave Imager Sounder (SSMIS) data. Markus and Cavalieri (2000) applied the NT algorithm to the 85 GHz band for SIC retrieval which is called the NT2 (Enhanced NSAS Team) algorithm. Kaleschke et al. (2001) proposed the ARTIST Sea Ice (ASI) algorithm and applied it to Advanced Microwave Scanning Radiometer–EOS (AMSR-E) data to obtain information on SIC (Spreen et al., 2008). Based on the ASI algorithm, Hao and Su (2015) developed the Dynamic Tie-Point ASI (DT-ASI) algorithm from AMSR-E data. Wu et al. (2019) enhanced the ASI algorithm by using the 19 GHz polarization difference to modify the 91 GHz polarization difference, which was then substituted into the ASI algorithm to calculate SIC. Tonboe et al. (2016) from AMSR2 data using the OSHD (OSI SAF Hybrid Dynamic), namely, a fusion algorithm of Bristol and Bootstrap. Also based on AMSR2 data using the TUD (Technical University of Denmark) algorithm (Lavelle et al., 2016). Based on the polarization ratio of the vertical polarization channel BTs at 18.7 GHz and 36.5 GHz, Zhang et al. (2013) developed a simple double-bias proportionality (DPR) algorithm from AMSR-E data. Table 1 lists the relevant information of the main SIC products based on these algorithms.

The National Satellite Meteorological Center (NSMC) released a SIC product with a resolution of 12.5 km based on the NT2 retrieval algorithm from the Microwave Radiation Imager (MWRI) data carried by FengYun-3B (FY-3B), a new-generation polar-orbiting Chinese meteorological satellite. Wang et al. (2018) compared the FY-3B SIC product and AMSR-E SIC from NSIDC for July to September, 2011, and verified SIC using MODIS data, finding a mean difference and root mean square of 9.78% and 19.53%, respectively. The accuracy of the FY-3B/NT2 provided is significantly lower than that of international products and the SIE is too large. Therefore, improvement of the quality of SIC retrieved by FY-3B satellites is necessary. Current approaches to improving sea ice concentration of FY-3B include cross-calibration of brightness temperature data, the introduction of other datasets for correction, and the use of different algorithms (Zhai et al., 2017; Wu et al., 2020; Tang et al., 2020). In recent studies, different algorithms have been applied to FY-3C or FY-3D to retrieve new SIC data, which are significantly improved compared with international products (Liu et al., 2020; Wu et al., 2020). Among these researches, no one has applied the DT-ASI algorithms to FY-3B satellites, and the amount of sample data selected in comparison is not systematic enough.

FengYun Meteorological Satellite is an important member of the globally integrated observation system, needs to find more applications to make further improvement of the satellite and optimize the data utilization nationally and internationally. Although the observation frequency of the FY-3B microwave radiometer is similar to that of the US DMSP/SSMIS, it has the potential to become the main data source for polar sea ice observations. However, there are still few sea ice concentration products based on FY-3B/MWRI. So the application of better algorithms to retrieval can not only increase the richness of data but also improve the accuracy. In this paper, we apply the DT-ASI algorithm to the FY-3B/MWRI to obtain 12.5 km resolution SIC data and compare the results with some similar products such as FY-3B/NT2, AMSR2/DT-ASI, AMSR2/ASI. Then we use MODIS visible-light data as the reference to verify the accuracy of new SIC results. Besides, the land spillover correction is used to reduce the erroneous SICs along the coastlines adjacent to open water. Finally, we provide a summary and discussion about this work.

2 Data and method

Dual-polarization BT at the 89 GHz channel from FY-3B/MWRI acquired from the NSMC (http://www.nsmc.org.cn) over a time span from November 18, 2010 to August 19, 2019 are used to retrieval SIC of 12.5 km resolution in this paper. BT data at 18.7 GHz, 23.8 GHz, and 36.5 GHz vertical channels are used for weather filters. The details of the algorithm will be given in Section 3.1. For climate research, calibration and correction of satellite data from different sensors are necessary to obtain accurate and consistent geophysical data (Cavalieri et al., 1999).

Although the channels of AMSR-E and MWRI are the same (Yang et al., 2012), there are system deviations for different sensors. Chen et al. (2021) cross-calibrated the brightness temperature data of the 10 channels corresponding to the two sensors on the up and down channels by conducting the monthly bias of each channel of MWRI and AMSR-2 in the study area, and then analysed the monthly bias between sea ice area and open water. We used this cross-calibration method to obtain all grid MWRI data after calibration with AMSR2.

Comparative data from similar products include the following. The University of Bremen, using the ASI algorithm, released an SIC product with a spatial resolution of 6.25 km, based on the 89 GHz channel of the AMSR2 data (https://www.uni-bremen.de/). The NSMC, using the NT2 retrieval algorithm, released an SIC product with a spatial resolution of 12.5 km. The Ocean University of China, using the DT-ASI algorithm, released an SIC product with a spatial resolution of 6.25 km based on the 89 GHz channel of the AMSR2 data (http://coas.ouc.edu.cn/pogoc/).

Table 1. Algorithms, data sources, resolutions, and time ranges of the main products for Arctic SIC

Algorithm	Data source	Issued	Resolution/km	Time range
Bootstrap	SMMR/SSM/I/SSMIS	National Snow and Ice Data Center (NSIDC)	25	1979 to present
	AMSR-E/AMSR2	University of Bremen (UB)	12.5	2002–2011; 2012 to present
Enhance NSAS Team (NT2)	AMSR-E	National Snow and Ice Data Center (NSIDC)	12.5	2002–2011
	MWRI	National Satellite Meteorological Center (NSMC)	12.5	2011–2019
	AMSR2	Japan Aerospace Exploration Agency (JAXA)	10	2012 to present
OSI SAF Hybrid Dynamic(OSHD)	SSMIS	European Organisation for the Exploitation of Meteorological Satellites (EUMETSAT)	10	1979 to present
	AMSR2		10	2012 to present
Technical University of Denmark (TUD)	AMSR2	European Organisation for the Exploitation of Meteorological Satellites (EUMETSAT)	10	2012 to present
Dual-Polarized Ratio (DPR)	AMSR-E/AMSR2	Ocean University of China (OUC)	10	2002–2011; 2012 to present
ARTSIST Sea Ice (ASI)	AMSR-E/AMSR2	University of Bremen (UB)	6.25	2002–2011; 2012 to present
Dynamic Tie Point ASI (DT-ASI)	AMSR-E/AMSR2	Ocean University of China (OUC)	6.25	2002–2011; 2012 to present

The verification data was extracted from MODIS visible light data, obtained from the NASA website (https://ladsweb.modaps.eosdis.nasa.gov/). In this paper, the MODIS L1B data of band 1 (0.620–0.670 μm) at 250 m spatial resolution are used to obtain SIC, and the ice water identification method is the tie-point algorithm (Steffen and Schweiger, 1991; Cavalieri et al., 2010). The specific method will be described in Section 5.

To perform a point-to-point comparison between SIC with different spatial resolutions, an inverse distance weight (IDW) method was used to interpolate the two sets of SIC data to a grid of 12.5 km. The SIE of SSMI/NT2 obtained from the US National Snow and Ice Data Center (NSIDC), and the SIE and SIA of other products are calculated based on area files of different resolutions, only calculate areas where SIC is greater than 15%.

3 Sea ice concentration retrieval

3.1 *Application of DT-ASI algorithm*

The DT-ASI retrieval algorithm (Hao and Su, 2015), based on FY-3B/MWRI data, includes the following steps.

In the first step, the ASI algorithm based on fixed tie points (Spreen et al., 2008) obtains the initial SIC field C using the following equation:

$$C = d_3P^3 + d_2P^2 + d_1P + d_0, \tag{1}$$

where P is the polarization difference between the horizontal and vertical BTs at 89 GHz; d_3, d_2, d_1, and d_0 are obtained by solving equations for the conditions of the pure water point value P_0 and pure ice point value P_1. The initial values are as follows: $P_0 = 47$ and $P_1 = 11.7$; when $P > P_0$, C is assigned a value of 0% for seawater; when $P < P_1$, C is assigned a value of 100% for sea ice.

The second step is to calculate the new daily tie point values. The daily average values of P_0 and P_1 under true atmospheric circumstances are calculated without using any weather filter. P_0 is the average of the 89 GHz polarization difference in all grid points without ice in the region of 53°–75°N; P_1 is the average of the 89 GHz polarization difference of all grid points where the weather-filtered SIC is greater than 95% in the region of 85°–90°N. Because the MWRI data has a larger hole than AMSR-E in the center of the North Pole, the selection range of ice point values is smaller. To determine the values of the open water tie point, the vertical polarization BT ratios of the 18.7 GHz and 36.5 GHz channels are introduced as a criterion (Zhang, 2012). Using the statistics of P_0 and P_1 as initial values, the BT polarization difference P is calculated again using the ASI algorithm, and the new FY-3B/MWRI SICs are obtained based on Eq. (1).

The third step is weather filtering. Due to the influence of abnormal atmospheric processes, some errors will occur on the open water surface, which will lead to false sea ice retrievals. It is necessary to introduce weather filters to deal with these errors. Hao and Su (2015) used two types of weather filters (Gloersen and Cavalieri, 1986).

The gradient ratios of GR $(36, 18)$ and GR $(23, 18)$ were used for judgment, and $\mathrm{GR}(X, Y) = [\mathrm{TB}(X, \mathrm{V}) - \mathrm{TB}(Y, \mathrm{V})] / [\mathrm{TB}(X, \mathrm{V}) + \mathrm{TB}(Y, \mathrm{V})]$ can be used to filter the false sea ice generated by clouds and water vapor, where X and Y are different frequency of BT andV stands for vertical channel. The threshold values are 0.045 and 0.04 respectively, which at least keeps all SICs at least 15% above. We use these two weather filtering methods (Gloersen and Cavalieri, 1986) and criteria to process the newly obtained FY-3B/MWRI SIC.

3.2 *Land spillover correction*

Limited by the wide diameter of the antenna, MWRI BT can detect relatively weak ground echo signals (Parkinson, 1987; Zhai et al., 2017). This makes it difficult to distinguish sea ice from land near the shore, which affects SIC products. To solve this problem, NSIDC SIC data has been introduced to identify pixels near the coastline. Liu et al. (2020) used the microwave scanning radiometer BT data from FY-3C to perform SIC retrieval in the polar region and used the minimum concentration template to remove land pollution effects. Similarly, in the FY-3B/DT-ASI SIC obtained by our retrieval, the land coverage and ocean coverage could not be distinguished. A land mask was applied to the ice concentration maps and adopted the technique of land spillover correction to deal with this problem. The errors in sea ice in the marginal area of the FY-3B SIC were corrected according to steps 1–3 of the land spillover correction method issued by the National Snow and Ice Center (Markus and Cavalieri, 2009). The specific steps of the algorithm are as follows:

(1) Classify all meshed pixels according to distance from the shoreline. Water points directly adjacent to the shoreline are set to 1. Outer boundary points are set to 2 and 3, respectively, and open water points and points adjacent to points with values of 2 and 3 are set to 0. Land locations close to the shoreline are set to 4, and points far from the shore are set to 5.

(2) Use a 7×7 window (about 87.5 km×87.5 km) to judge the concentrations of points with values of 1 and 2. Points with a value of 0 or 3 are not included in the detection range.

(3) Determine whether all points with a value of 3 in each window are open water. If they are, then the SIC of the points corresponding to points with values of 1 and 2 in the window are set to 0; otherwise, the concentration values of the corresponding points do not change.

Through the land spillover correction, the errors in sea ice near the shoreline were corrected to a major degree, and the SIE was also significantly corrected. This is important for shipping and resource utilization in the Arctic region, e. g., the Northwest Passage, which runs from Greenland through the Canadian Arctic Archipelago to the northern coast of Alaska, can greatly shorten the route between the Atlantic and the Pacific and has important economic value. Sea ice of the Canadian Arctic Archipelago is the key to the navigation time in summer, but PM products are subject to deviations due to low resolution. So, it is necessary to apply the land spillover method in these areas. Figure 1 shows the regional SIC distribution in the Canadian Arctic Archipelago before and after land spillover correction and the local satellite imagery on August 8, 2016. It shows that the land spillover method does not change the distribution of sea ice in large areas and only corrects the sea ice in small areas located at the edge of land (Figs 1a and b). Comparisons with satellite imagery (Fig. 1c) show that there is little sea ice for navigation in the western and southern ocean passages, consistent with the results in Fig. 1b. Most of the SIC in this area was greater than 15%, which would affect the calculation of SIE. Then, we calculated that the SIE values of this region (66°–76°N, 70°–130°W) were 17.7×10^4 km^2 and 14.3×10^4 km^2 respectively before and after using this method, which decreased by 19.2%. Therefore, the land spillover method can effectively correct a large number of misjudged sea ice, downgrade the differences between different data sets, and guide the determination of navigation time in the local sea area. Meier et al. (2015) pointed out the land spillover issue can add false ice along the coast, particularly during summer. In the Arctic Ocean during wintertime, the landfast ice covers almost the entire coastal area, so we improved to use the land spillover method from July 1st to December 1st every year, because most of the sea ice is not connected to land during this period.

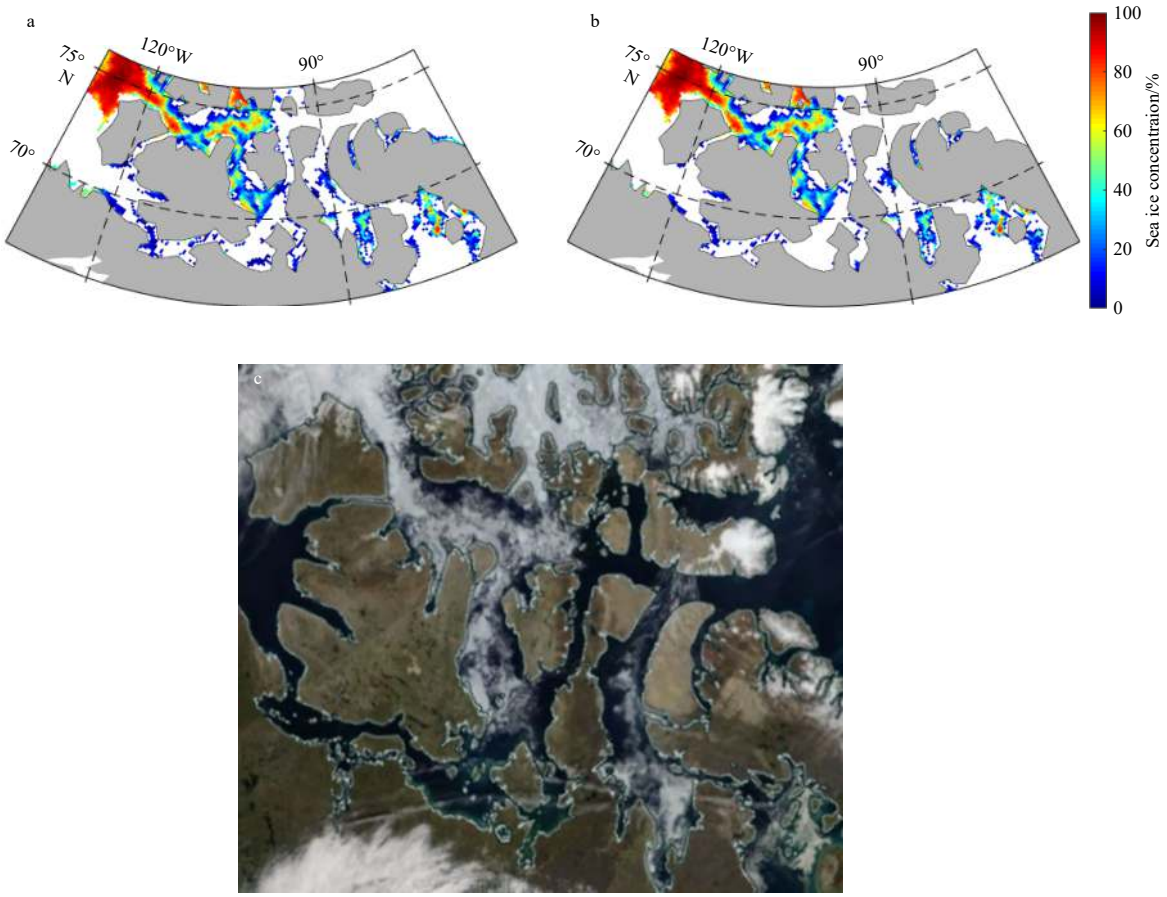

Fig. 1. Sea ice concentration in the Canadian Arctic Archipelago on August 8, 2016. a. Without land spillover correction, b. with land spillover correction, and c. satellite imagery from NASA Worldview (https://worldview.earthdata.nasa.gov) .

4 Results and comparison

By applying the DT-ASI retrieval algorithm to the FY-3B/MWRI data, daily Arctic SIC data was obtained from November 18, 2010 to August 19, 2019 with a spatial resolution of 12.5 km. Obtained 3 156 data, of which 3 120 valid data. The effective rate reached 98.9%. We compared results of FY-3B/DT-ASI with retrieval data using similar ASI algorithms, as well as with FY-3B/NT2 data. SIE and SIA from these datasets were also compared.

4.1 *Comparison of SIC with other data derived from similar algorithms*

In this section, we compare our results with SIC products obtained by the University of Bremen (UB) and the Ocean University of China (OUC), expressed as AMSR2/ASI and AMSR2/DT-ASI. Both data have a resolution of 6.25 km.

All three sets of results show a similar seasonal cycle of the SIC. We compare the monthly average Arctic SIC of the three products for eight years. For example, Fig. 2 and Fig. 3 give the SIC distributions of the three datasets for March and September. In all three sets of results for both March and September, the monthly average distribution of SIC is very similar and the values are very close, especially the two sets of results of AMSR2. The differences between FY-3B/DT-ASI and the two AMSR2 results appear mainly in the ice edge area. For March, the differences appear primarily in the Sea of Okhotsk and the ice margin zone of the North Atlantic, with smaller values in the FY-3B data. However, in September, FY-3B/DT-ASI is higher than AMSR2/DT-ASI, especially in the East Greenland Sea, and lower than AMSR2/ASI. The main differences are still in the ice margin zone along the Northeast Passage, which facilitates navigation of the Arctic in summer. Compared with the two AMSR2 products, FY-3B/DT-ASI can describe the lower SIC in the edge and the hole at the North Pole is bigger.

In summary, the three types of SIC obtained by similar ASI algorithms resemble each other better in March than in September. The main reason for the difference between FY-3B/DT-ASI and the two AMSR2 SIC products is the difference in the size of footprints.

4.2 *Comparison of SIC with FY satellite products*

In this section, FY-3B/DT-ASI SICs are compared with the SIC products distributed by NSMC, which are based on the NT2 algorithm, referred to here as FY-3B/NT2. In most cases, our results are lower than those from FY-3B/NT2. For example, Fig. 4 shows that the two SICs differ greatly in the sea ice margin area and at the edge of the land. SIC from FY-3B/DT-ASI is higher in the north and east of the Beaufort Sea and the marginal ice zone of the Barents Sea and lower in most of the Arctic Ocean, especially in the Greenland Sea and the Baffin Bay. The large difference in SIE values between the two sets of FY-3B data (11.19×10^6 km^2 from FY-3B/DT-ASI and 13.07×10^6 km^2 from FY-3B/NT2) comes mostly from the region close to the coast.

The daily spatial average SIC difference and the monthly spatial average SIC difference between FY-3B/DT-ASI and FY-3B/NT2 are shown in Figs 5a and b. Overall, the daily spatial average SIC from our results is smaller than that from FY-3B/NT2,

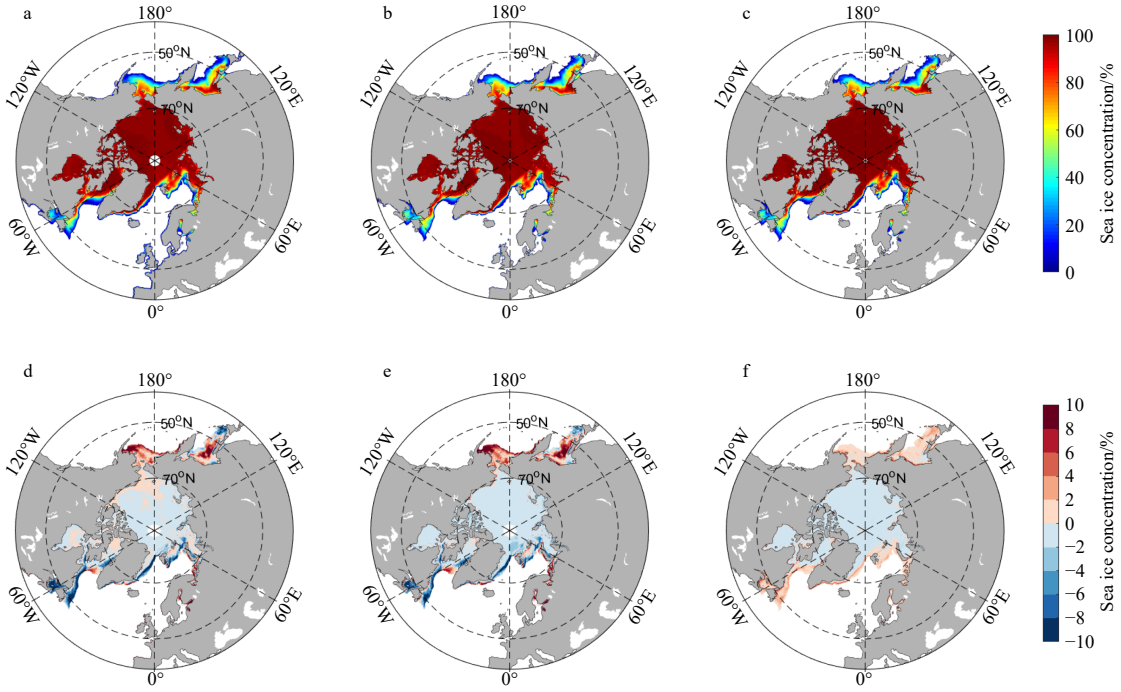

Fig. 2. Monthly averaged sea ice concentration in March. a. FY-3B/DT-ASI, b. AMSR2/DT-ASI, c. AMSR2/ASI, and d-f. sea ice concentration differences between FY-3B/DT-ASI and AMSR2/DT-ASI, FY-3B/DT-ASI and AMSR2/DT-ASI, and AMSR2/DT-ASI and AMSR2/ASI.

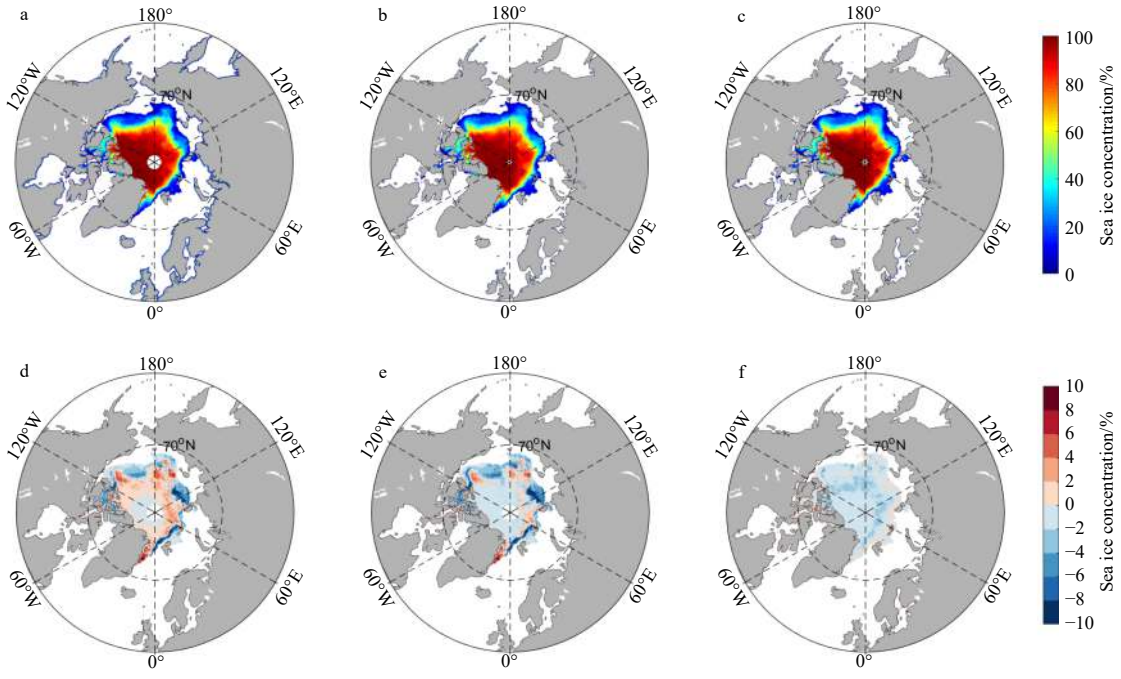

Fig. 3. Monthly averaged sea ice concentration in September. a. FY-3B/DT-ASI, b. AMSR2/DT-ASI, c. AMSR2/ASI, and d-f. sea ice concentration differences between FY-3B/DT-ASI and AMSR2/DT-ASI, FY-3B/DT-ASI and AMSR2/DT-ASI, and AMSR2/DT-ASI and AMSR2/ASI.

with an average of –2.31%. Several abnormally large differences are due to the SIC polluted by the lack or excessive orbital data (Fig. 5a). From Fig. 5b, it is not difficult to find that the difference of monthly averaged SIC from 2011 to 2018 is larger in the first half-year than in the second half-year.

4.3 *Comparison of SIE and SIA*

Two parameters that proved a quantitative evaluation of the large-scale changes and trends of sea ice are SIE and SIA. The usual method for calculating SIE is the sum of the areas of all grid cells with SIC greater than 15%, and SIA is the sum of the

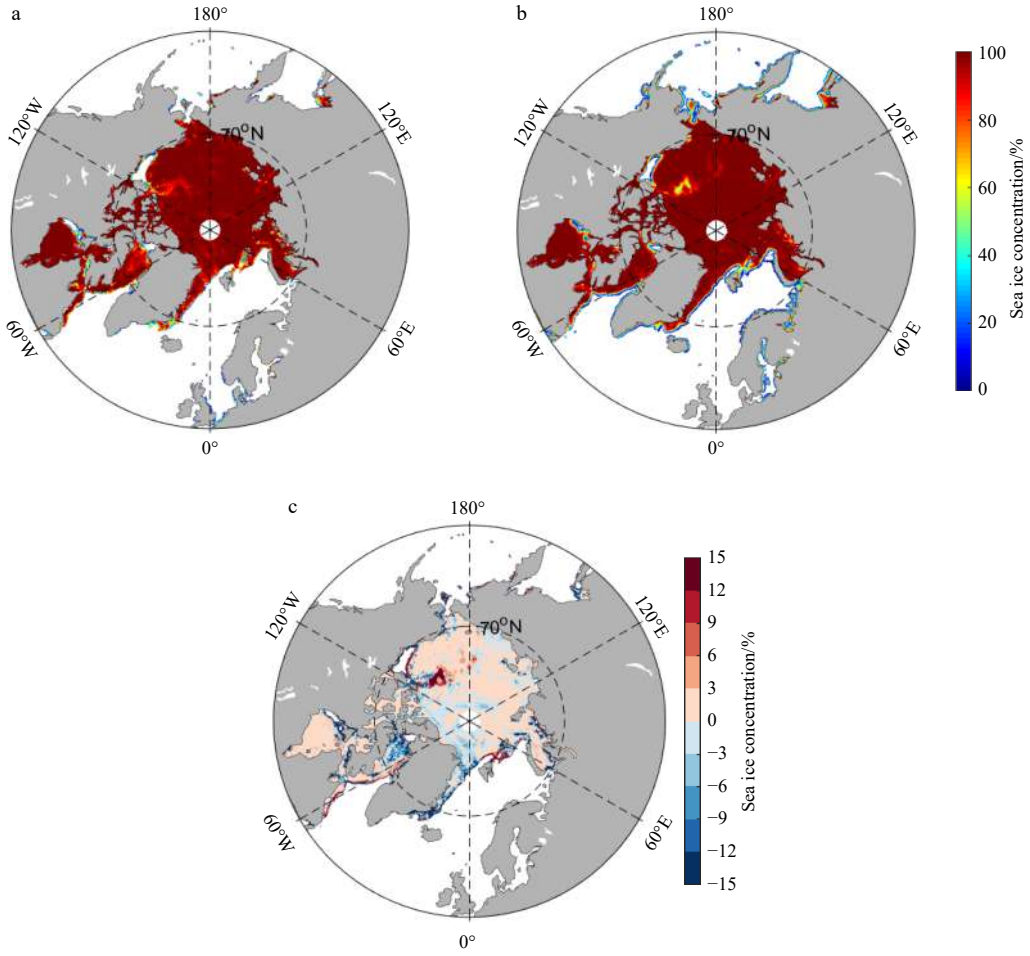

Fig. 4. Arctic sea ice concentration from FY-3B/DT-ASI (a) and FY-3B/NT2 (b) on May 14, 2016 as well as their difference (c).

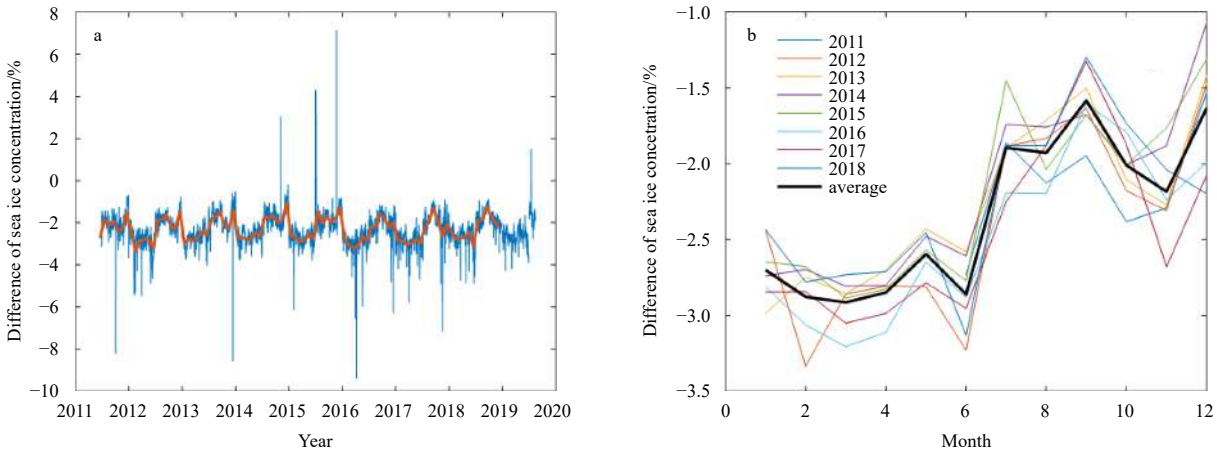

Fig. 5. Time series of the daily spatial averaged difference of FY-3B/DT-ASI and FY-3B/NT2 (a), and the monthly spatial averaged sea ice concentration difference of FY-3B/DT-ASI and FY-3B/NT2 (b). The red line in a represents the monthly mean.

products of the area of each grid unit and the corresponding SIC. Here, we compare daily SIEs obtained from SICs from five datasets (FY-3B/NT2, NSMC; FY-3B/DT-ASI, OUC; AMSR2/DT-ASI, OUC; AMSR2/ASI, UB; SSMI/NT2, NSIDC). For SIA, we compare results from four datasets, excluding SSMI/NT2, which does not provide SIA data.

A comparison of climatological daily SIEs for 2012–2018 is presented in Fig. 6a. It can be seen directly that the SIE time series of all these datasets exhibit obvious seasonal changes, and some SIE fluctuations due to changes in weather scale can also be observed. The yearly average SIEs are 11.94×10^6 km^2, 10.52×10^6 km^2, 10.51×10^6 km^2, 10.29×10^6 km^2, 10.5×10^6 km^2, and 10.3×10^6 km^2 for FY-3B/NT2, AMSR2/DT-ASI, SSMI/NT2, AMSR2/ASI, FY-3B/DT-ASI(V0), and FY-3B/DT-ASI, respectively.

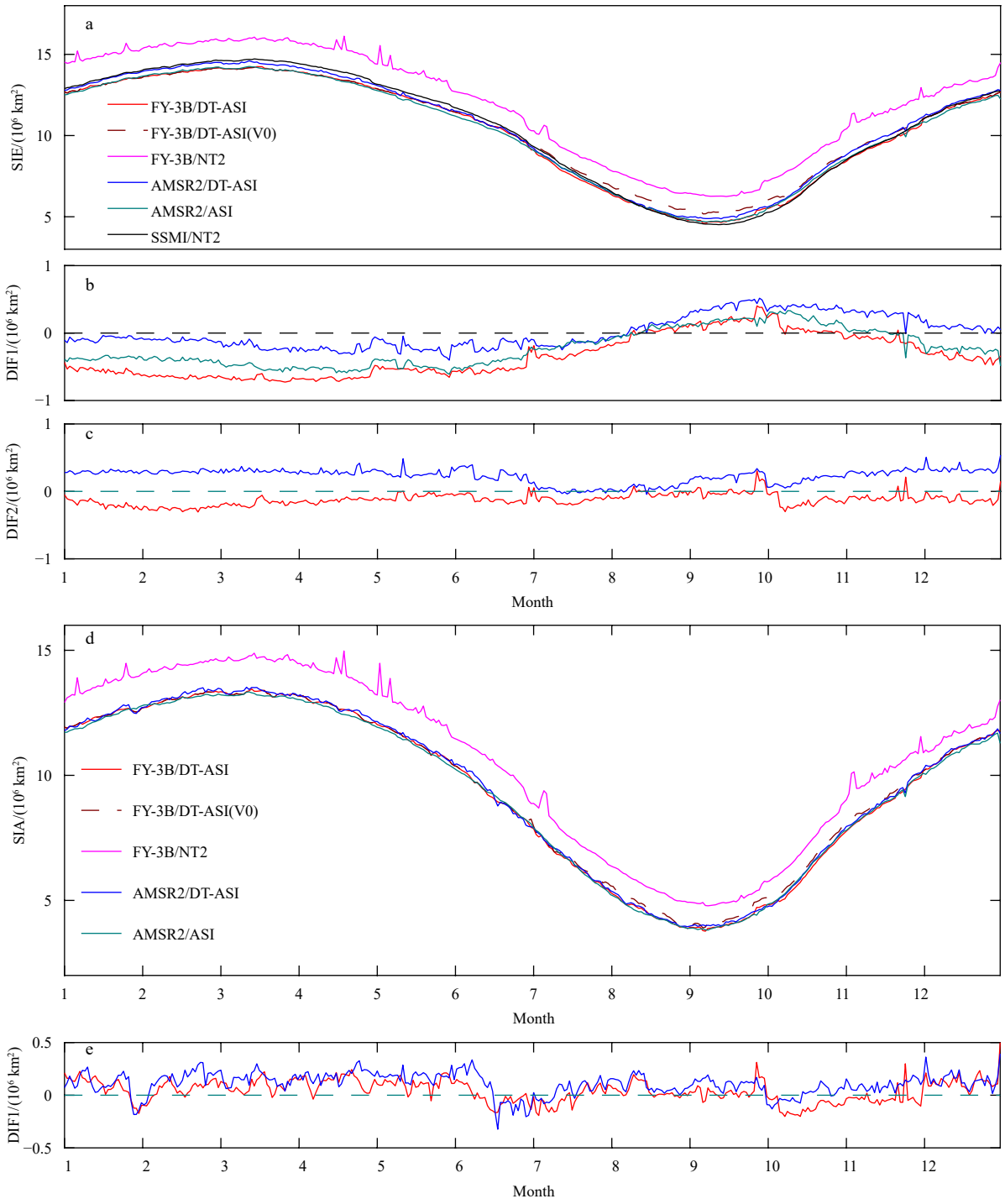

Fig. 6. Time series of comparison of sea ice extent (SIE) from different datasets (a), differences of SIE with those from SSMI/NT2 (b, DIF1), differences of SIE with those from AMSR2/ASI (c, DIF2), time series of comparison of sea ice area (SIA) from different datasets (d), and differences of SIA with those from AMSR2/ASI (e, DIF1). The color coding of the lines in the different plots are the same as for the respective SIE and SIA plots. The brown dotted line is FY-3B/DT-ASI (V0) which represents without using the land spillover method.

FY-3B/DT-ASI(V0) stands for our SIC result without using the land spillover method. Therefore, the reduction of SIE by the algorithm accounted for 87.9%, and the land spillover accounted for 12.1%. The SIE from the FY-3B/NT2 data is much greater than that from the other data. Among the three datasets of results obtained using the ASI and DT-ASI algorithm, in comparison with SSMI/NT2, the absolute biases of the SIE are all within 0.8× 10^6 km^2(Fig. 6b). From January to July, their SIEs are less than those from SSMI/NT2 (with the bias between AMSR2/DT-ASI and SSMI/NT2 being the smallest), whereas from September to November, larger than SSMI/NT2, so the deviation varies with the seasons and exhibits similar fluctuations. As shown in Fig. 6c, the SIE of FY-3B/DT-ASI is smaller than AMSR2/ASI, and the SIE of AMSR2/DT-ASI is higher than AMSR2/ASI. Overall, the three

SIE results of the ASI algorithm are very close in summer.

A comparison of SIAs is shown in Figs 6d and e. The time series of SIA from the four SIC datasets are similar to the SIE time series. The SIA from the FY-3B/NT2 data is much greater and the FY-3B/DT-ASI results are closer to the other two AMSR2 datasets. The yearly average SIAs are 10.60×10^6 km^2, 9.49×10^6 km^2, 9.38×10^6 km^2, 9.51×10^6 km^2, and 9.42×10^6 km^2 for FY-3B/NT2, AMSR2/DT-ASI, AMSR2/ASI, FY-3B/DT-ASI(V0), and FY-3B/DT-ASI, respectively. The reduction of SIA by the algorithm accounted for 92.4%, and the land spillover accounted for 7.6%. Comparison of FY-3B/DT-ASI and AMSR2/DT-ASI with AMSR2/ASI shows that the differences between -0.5×10^6 km^2 and 0.5×10^6 km^2. The changing trends of the two biases are consistent, which is the opposite of SIE.

Figures 7a–d give monthly average SIE and SIA time series from four SIC datasets for March and September from 2011 to 2018. The inter-annual changes of SIAs and SIEs in the four SIC datasets in March and September were basically the same. Both reached their lowest on record in September 2012. The SIEs and SIAs from FY-3B/NT2 are clearly larger than those from the other three SIC datasets. The SIEs from three used ASI algorithm datasets are lower for March and higher for September than SSMI/NT2. The SIE and SIA for March from the FY-3B/DT-ASI are the smallest, and very close to AMSR2/ASI in September.

5 Validation with MODIS SIC

In previous studies, high-resolution satellite image data has generally been used to verify the SICs obtained from PM data by different methods. For example, Zhao and Ren (2000) proposed an intensity ratio threshold zone method in which a threshold based on ice-water discrimination is used to calculate the proportion of ice in the corresponding grid (Wiebe et al., 2009; Ye et al., 2011). The SIC in the visible light image is thereby obtained. In this study, we used the tie-point algorithm (Steffen and Schweiger, 1991; Cavalieri et al., 2010) to extract SICs from MODIS.

Differences mainly occur in marginal ice regions (Cavalieri et al., 2010). Therefore, we select 58 cloud-free case scenes with 250 m resolution visible light channel data provided by MODIS onboard the AQUA satellite from February to July during 2012 and 2019. The distribution of the location of these case scenes (Fig. 8) covers almost all marginal sea areas in the Arctic (except the Barents Sea).

SIC was retrieved from band 1 of MODIS L1B visible light (MYD02Q KM) data. Select the sample with an area of 100 km × 100 km, and each window contains 160 000 pixels. Generally, there are two peaks in the probability density functions (PDF) histogram of the top-of-the-atmosphere (TOA) reflectance: the value of the water point A_w and the value of the ice point A_i. Then use the tie-point algorithm to calculate the SIC in each pixel. When the reflectance was greater than A_i, SIC was set to 100%; when the reflectance was less than A_w, SIC was set to 0; when the reflectance was between A_w and A_i, the value of SIC was linearly scaled between 0 and 1.

Figure 9 shows three of the 58 samples (10, 29, and 34), corresponding to the colored frames in Fig. 8. Their acquisition times were June 5, 2013, June 5, 2017, and July 12, 2017, respectively. The three samples represent three types: (1) mainly broken ice with a small size, but relatively high SIC; (2) the sea ice edge zone, including large pieces of sea ice and with a relatively high proportion of seawater; (3) pack ice with melt ponds, with a high SIC.

We then projected the high-resolution MODIS SIC onto the low-resolution SIC data grid (6.25 km × 6.25 km and 12.5 km × 12.5 km). Figure 10 shows the SIC distribution from MODIS and the retrieval results from FY-3B/DT-ASI, FY-3B/NT2, AMSR2/DT-ASI, and AMSR2/ASI. The results show that among the three samples, the SICs from AMSR2/DT-ASI and AMSR2/ASI give descriptions of the distribution characteristics of sea ice that are closer to those from MODIS (Figs 10b1–b3) owing to their higher spatial resolution. FY-3B/NT2 (Figs 10c1–c3), with a resolution of 12.5 km, generally gives a higher SIC than MODIS. It cannot clearly reproduce the distribution characteristics of Sample 29 (Fig. 10c2). Our FY-3B/DT-ASI results with a resolution of 12.5 km (Figs 10d1–d3) generally have lower SICs, with distribution characteristics more like those from MODIS results than FY-3B/NT2.

For Sample 10, SIC from MODIS (Fig. 10a1) with a spatial resolution of 250 m can characterize narrow open water. Limited by spatial resolution, PM results cannot recognize tiny open water areas in detail, but still reveal the water and low SIC value in the upper right area, while FY-3B/NT2 gives a higher SIC than that obtained from the other datasets.

For Sample 29, the sea ice and seawater points account for almost half each. SICs retrieved from the two AMSR2 datasets (Figs 10e2 and f2) better reflect of the actual situation, and the position of the sea ice edge is basically the same as that of MOD-

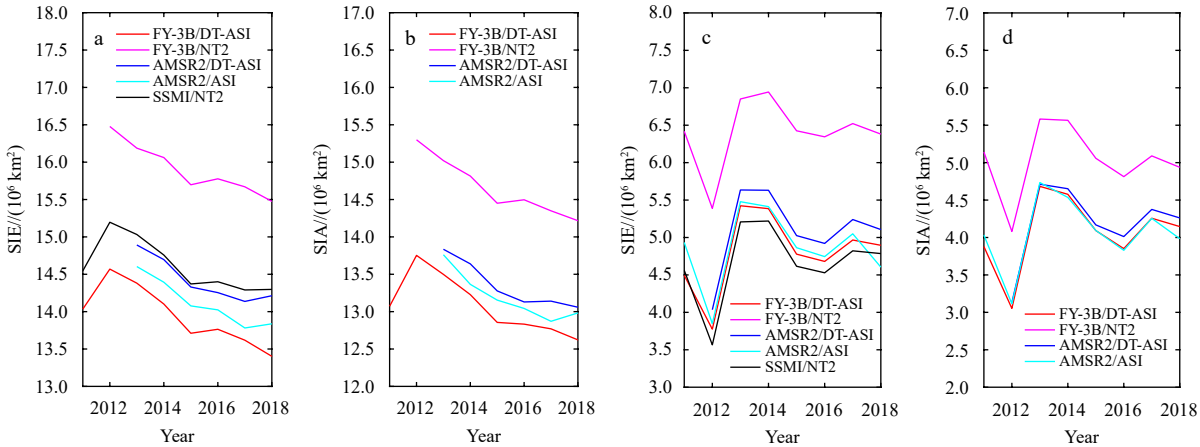

Fig. 7. Monthly averaged sea ice extent (SIE) and sea ice area (SIA) of different datasets in March and September. a. SIE for March, b. SIA for March, c. SIE for September, and d. SIA for September.

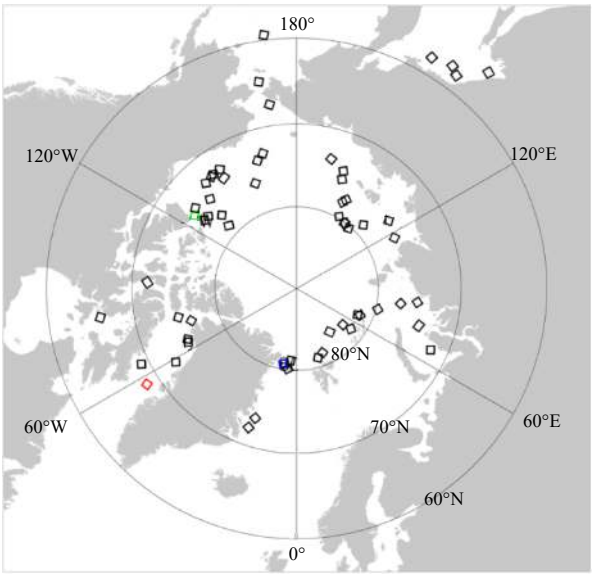

Fig. 8. Selection of MODIS broadband top of the atmosphere reflectance images. The red, green, and blue squares show the positions of samples 10, 29, and 34, respectively.

IS (Fig. 10b2). The FY-3B/DT-ASI retrieval result can also accurately capture the edge of ice and water, but the high SIC area is smaller than the MODIS result. The FY-3B/NT2 result has the largest difference from the actual value, and the range is much larger than that from MODIS.

For Sample 34, FY-3B/DT-ASI, AMSR2/DT-ASI, and AMSR2/ASI all give distributions of SIC that adequately represent the sample SIC, although the first one with a lower value (Fig. 10c3) while the last one (Fig. 10f3) with a higher value than that from MODIS. FY-3B/NT2 SIC values are much higher than those from MODIS and almost with a uniform distribution.

Among the three samples, we could see that the results of the two high-resolution SICs are better than the results of the 12.5 km SIC. FY-3B/NT2 results in the largest deviation. Although FY-3B/DT-ASI cannot represent the details of the distribution characteristics, compared with the results of MODIS, both the value and the rough distribution are acceptable.

We acquired spatially averaged SICs for the 58 selected regions from five different kinds of SICs, as shown in Fig. 11. All sample results are ordered from 2012 to 2019 by date. The average SIC of MODIS, FY-3B/DT-ASI, FY-3B/NT2, AMSR2/DT-ASI, and AMSR2/ASI are 65.0%, 65.4%, 81.5%, 64.5%, and 64.7%, respectively. The SICs from the ASI algorithms are consistent with those from MODIS, while those from FY-3B/NT2 are the largest. In terms of the averaged SIC from FY-3B/DT-ASI, 31 samples are greater and 27 samples lower than that from MODIS. And 62% of the samples have an average difference within 10%.

Wang et al. (2018) compared the SIC data of FY-3B/NT2 and AMSR-E and validated with MODIS, when the SIC was 95% or higher, the root mean square difference (RMSD) was significantly reduced. This indicates that the SIC difference fluctuates less in high-SIC areas. In the verification process, this paper also uses the method of statistical mean difference (MD), mean absolute difference (MAD) and RMSD of the sub-concentration to divide the MODIS retrieval SIC into three levels. The results are shown in Table 2. When SIC > 90%, FY-3B/NT2 has the best performance, and when SIC < 90%, FY-3B/NT2 has the largest difference. The MDs of the two AMSR2 products and FY-3B/DT-ASI are close to zero. The MAD of FY-3B/DT-ASI, FY-3B/NT2, AMSR2/DT-ASI, and AMSR2/ASI are 12.7%, 19.9%, 11.2% and 10.8%, respectively, and the distribution is similar to RMSD. Compared with that from FY-3B/NT2, the total MD, MAD and RMSD from FY-3B/DT-ASI are reduced by 16%, 1.5% and 8%, respectively. The results of the three levels show that RMSD increases significantly as the SIC decreases.

6 Summary and discussion

Sea ice concentration product from the Chinese FengYun satellites has been publicly available since 2011, and there have been a number of attempts to improve it (Zhai et al., 2017; Wu et al., 2020). In this paper, we apply the DT-ASI algorithm, which has been used in the GCOM-W1/AMSR2 sea ice concentration retrieval in Ocean University of China to the FY-3B/MWRI 89 GHz BT data to retrieve Arctic SIC. A new daily SIC dataset is obtained, covering 2010–2019. We also adopt the land spillover method to correct the SIC for contamination at the edge from July 1st to December 1st that has obvious improvements to SIE and SIA. By comparing with those from other PM SIC products and with MODIS visible light data, the main characteristics of our results can be summarized as follows:

(1) The SIC results retrieved by the DT-ASI algorithm from FY-3B/MWRI data show spatial distributions that are highly consistent with those from ASI and DT-ASI algorithms based on GCOM-W1/AMSR2 data. The SIC bias is larger in the marginal ice zone, and the deviations of the three sets of SIC results in September are larger than those in March. Our SIC results are lower than those from FY-3B/NT2 in most areas and the spatial

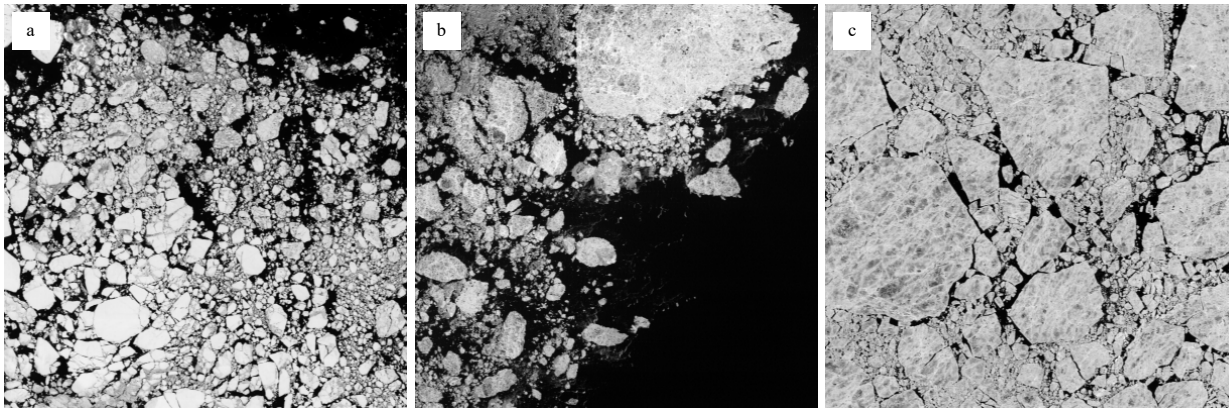

Fig. 9. MODIS broadband TOA reflectance images. a. Sample 10; b. Sample 29; and c. Sample 34.

average SIC bias is negative, with an average of –2.31%, and is bigger in the first half year than in the second half year. And the land spillover method can effectively correct the differences in SIC in the summer.

(2) Compared with FY-3B/NT2, FY-3B/DT-ASI has obvious improvements in SIE and SIA, and the average value is very close to that of several other released products. The yearly average SIE of FY-3B/DT-ASI is reduced by 1.65×10^6 km^2, of which the DT-ASI algorithm accounts for 87.9% and the land spillover method accounts for 12.1%. In some of the more complex coastal areas, the land spillover accounted for a greater proportion of improvement, such as the Northwest Passage. The SIAs and SIEs from all four SIC datasets exhibit the same interannual variations in March and September.

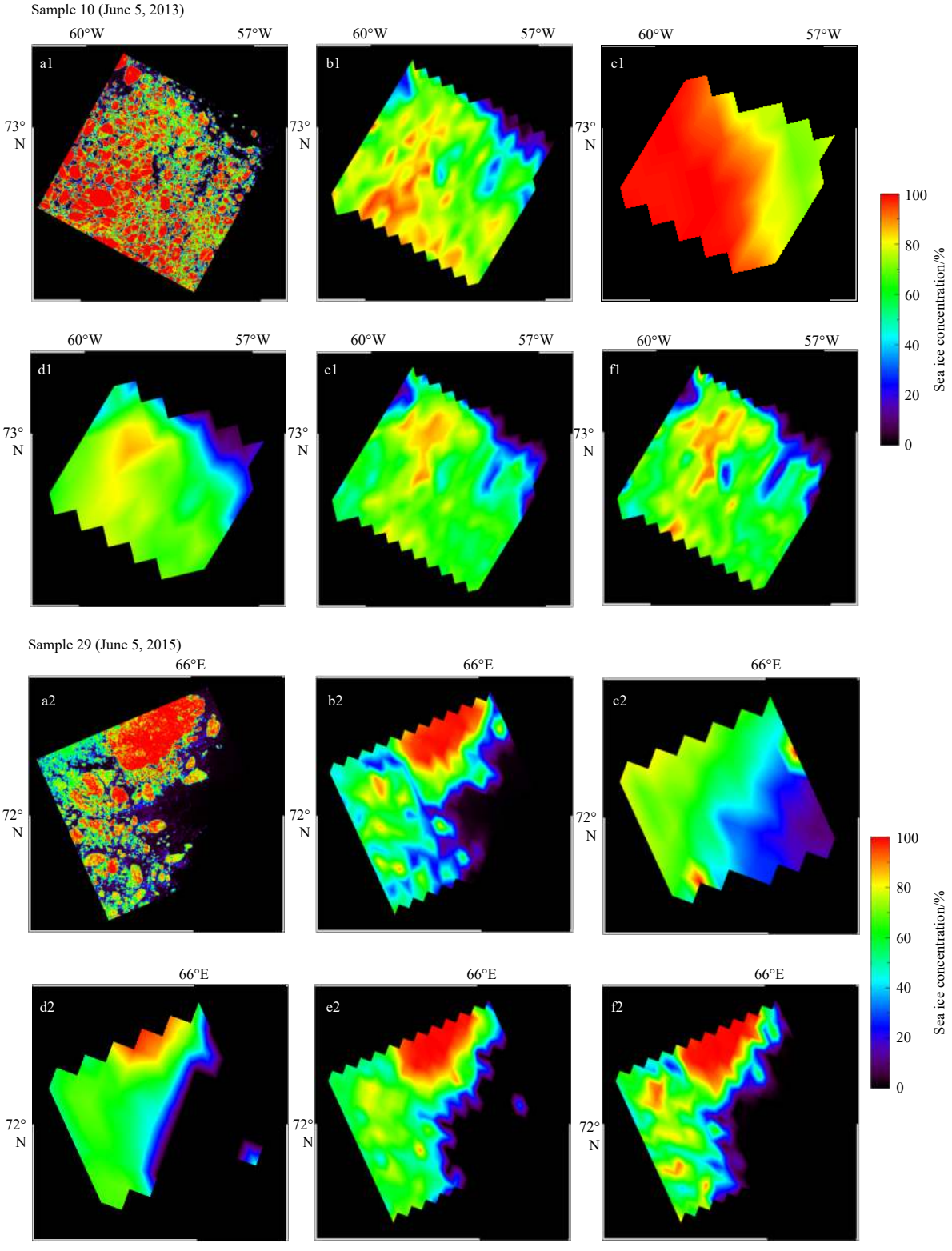

Fig. 10.

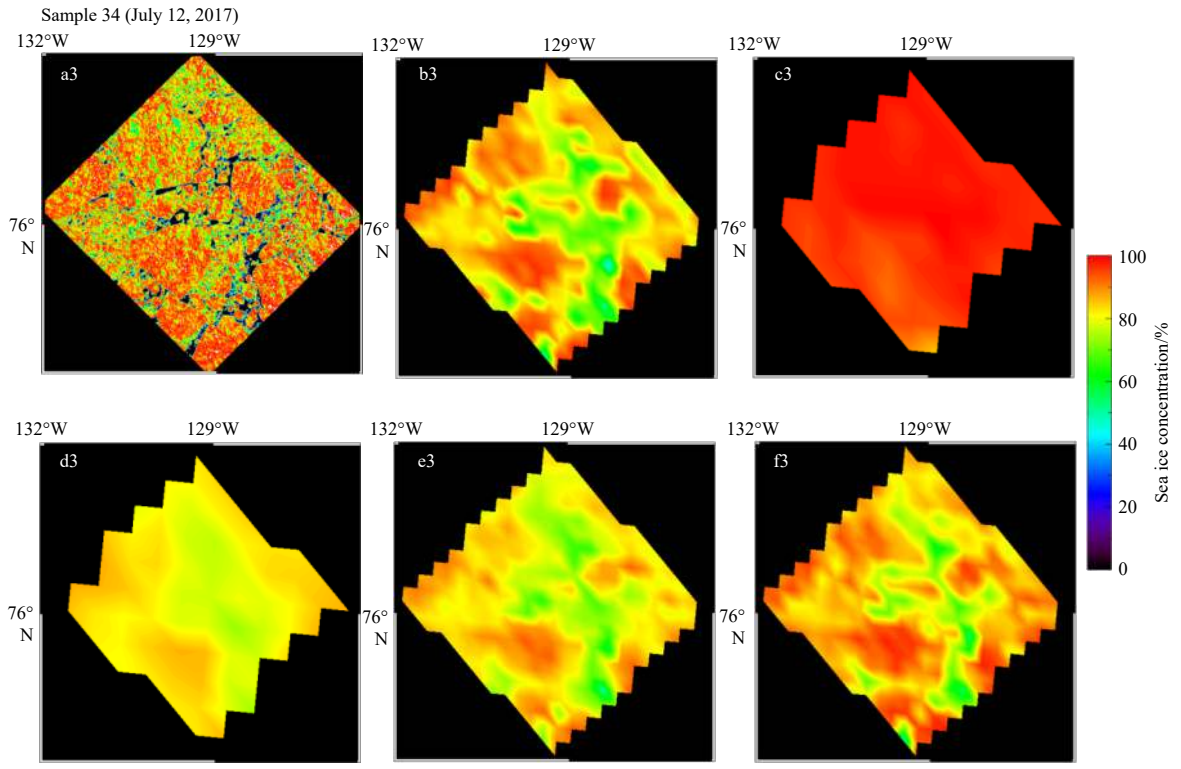

Fig. 10. Sea ice concentration (SIC) corresponding to the three selected samples. a. MODIS SIC with a resolution of 250 m, b. MODIS SIC with a resolution of 6.25 km, c. FY-3B/NT2 with a resolution of 12.5 km (NSMC), d. FY-3B/DT-ASI with a resolution of 12.5 km, e. AMSR2/DT-ASI with a resolution of 6.25 km, and f. AMSR2/ASI with a resolution of 6.25 km (UB).

(3) Compared with the SIC retrieved from 58 MODIS samples, the MD, MAD and RMSD of FY-3B/DT-ASI results were 0.5%, 12.7% and 17.2%, obviously lower than those from FY-3B/NT2. All PM products show that the inversion accuracy is better in areas with higher SIC, and when the SIC is lower than 0.6, the RMSD basically reaches 20%.

Our work has confirmed that the DT-ASI algorithm can be effectively applied to FY-3B/MWRI and got better SIC data based on this sensor in the Arctic. The corresponding FY-3B/MWRI SIC product has been released in Key Lab of Polar Oceanography and Global Ocean Change at Ocean University of China operationally since January 2019. The datasets can be obtained from the website (http://coas.ouc.edu.cn/pogoc/). We analyzed the contributions of SIE and SIA brought by algorithms alternative and using land spillover, proving that the application is very valuable. Compared the results of FY-3B/MWRI retrieval using the DT-ASI algorithm with the SIC from visible light with an MD of 0.5%, while using ASI algorithm was 5.029% (Wu et al., 2020). However, there are still some aspects that need further improvement. First, the algorithm is currently not very good at retrieving SIC in the marginal ice zone. Second, daily tie-points still exhibit discontinuities when the BT at 89 GHz is affected by clouds and water vapor during strong weather processes. An atmospheric correction model will need to be incorporated to deal with this problem. Third, Comiso and Kwok (1996) suggested that PM SIC algorithms often underestimate high-value SIC in the melting season in comparison with SAR and AVHRR data owing to the influence of melt ponds. However, they drew this conclusion from a statistical analysis of SAR and AVHRR results on sea ice using simple binary discrimination rather than by linear scaling of SIC. In addition, they assumed that grids with melt pond coverage could be taken as pure ice grids. However, in reality, this may not be appropriate for the estimation of radiation balance. Therefore, we believe that if the PM signal is affected by melt condition, this effect should be counted into the SIC calculation.

Although the land spillover method can effectively reduce the influence of land pixels that is associated with low spatial resolution in most cases, it still cannot reduce the uncertainty in areas with a complex shoreline. At present, Arctic navigation is a common concern of all parties in the world, and we will give more consideration to the role of the land spillover method. Liu et al. (2020) used the BT correction and the minimum SIC mask during summer to correct the FY-3C/NT2, and the results are highly consistent with the NSIDC product. But the minimum mask chosen does not represent the SIE for all years. Therefore, the land spillover method used in this study is based on SIC's daily search for judgment, which has greater flexibility. The results showed that the land spillover method improved SIE by 19.2%, which is higher than the average contribution of 12.1% of the whole Arctic. Therefore, the land spillover method can downgrade the differences between different data sets. It also shows the advantages of improving SIE in special regions.

The MODIS SIC is taken as the ground truth in this paper. However, MODIS results are also subject to errors (Wiebe et al., 2009). According to Figs 10a, and b, the downscaling process of the MODIS 250 m SIC onto 6.25 km grids reduced the SIC, leading to a certain degree of underestimation of SIC in the high-SIC grids and overestimation in the low-SIC grids.

There are two main reasons for the large SIE and SIA from the FY-3B/NT2 analysis. First, the SIC value was larger than the other PM SIC products. Second, errors in sea ice caused by land spillover near the shore boundary were not dealt with. However, if we take the melt surface ice as pure ice, and use a statistical method to calculate SIC from MODIS data, the SIC from FY-3B/

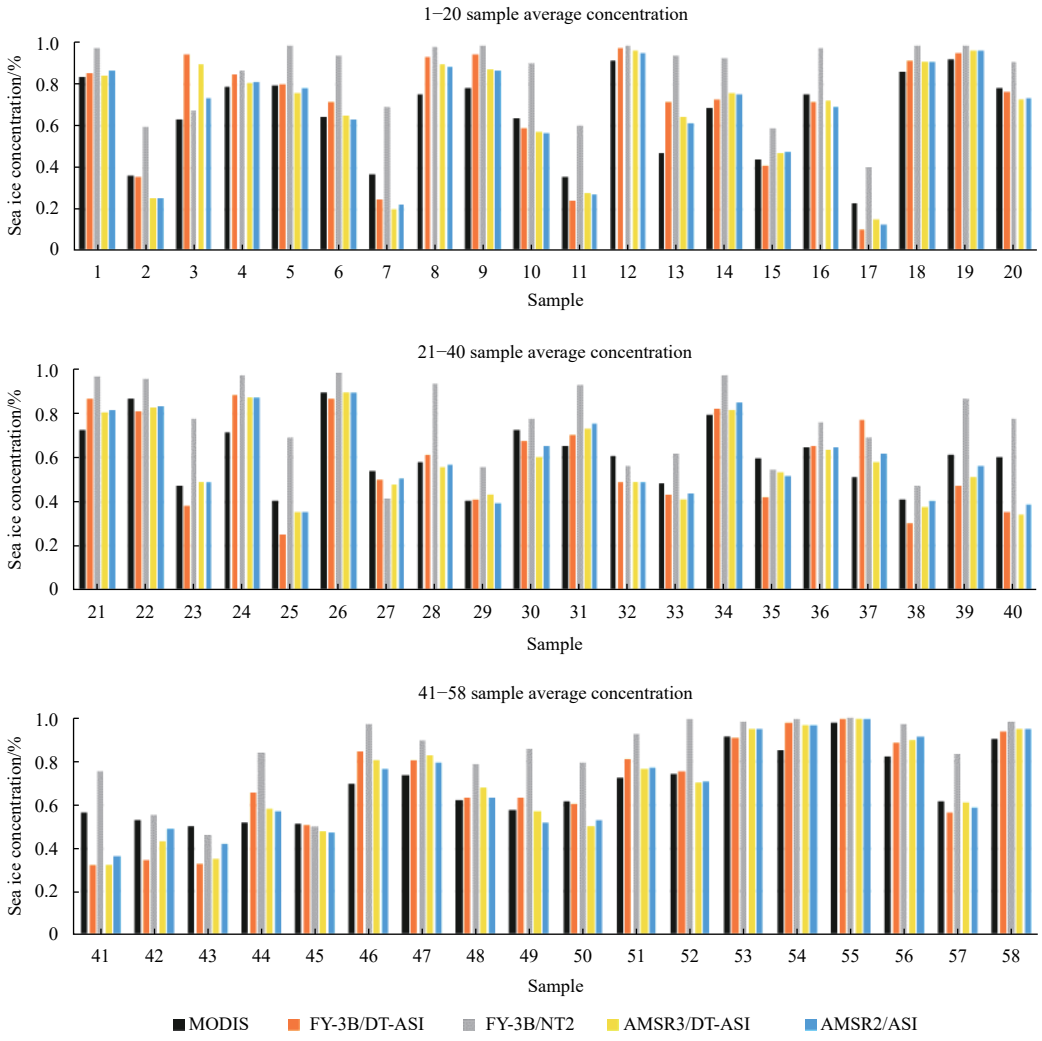

Fig. 11. Average sea ice concentration of 58 samples in different data.

Table 2. Statistical differences between the SICs from different data sets with MODIS (%)

		FY-3B/DT-ASI	FY-3B/NT2	AMSR2/DT-ASI	AMSR2/ASI
Total	MD	0.5	16.5	–0.9	–0.4
	MAD	12.7	19.9	11.2	10.8
	RMSD	17.2	25.2	14.8	14.7
SIC≥90%	MD	–6.4	0.78	–8	–4
	MAD	10.4	8.8	10.1	7.7
	RMSD	12.3	9.6	12.2	9.9
60%≤SIC <90%	MD	–2.3	10.5	–3.1	0.3
	MAD	14	15.3	13.6	12.6
	RMSD	17	17.4	16.4	15.7
SIC<60%	MD	6.3	33.6	4	1.4
	MAD	17.8	34.9	16	15.2
	RMSD	21.6	37.6	19.9	19.3

NT2 will have smaller errors compared with that from MODIS. Further validation needs to be done in the future.

Acknowledgements

We thank all the authors, reviewers and editor of this article for providing useful comments that have improved this research. The brightness temperature data are downloaded from the National Satellite Meteorological Center (http://www.nsmc.org.cn/NSMC/Home/Index.html).

References

Bjørgo E, Johannessen O M, Miles M W. 1997. Analysis of merged SMMR-SSMI time series of Arctic and Antarctic sea ice parameters 1978–1995. Geophysical Research Letters, 24(4): 413–416, doi: 10.1029/96GL04021

Cao Meisheng, Jin Rui. 2006. Monitoring sea ice concentration using remote sensing technique. Remote Sensing Technology and

Application (in Chinese), 21(3): 259–264
Cavalieri D J, Gloersen P, Campbell W J. 1984. Determination of sea ice parameters with the Nimbus 7 SMMR. Journal of Geophysical Research: Atmospheres, 89(D4): 5355–5369, doi: 10.1029/JD089iD04p05355
Cavalieri D J, Gloersen P, Parkinson C L, et al. 1997. Observed hemispheric asymmetry in global sea ice changes. Science, 278(5340): 1104–1106, doi: 10.1126/science.278.5340.1104
Cavalieri D J, Markus T, Hall D K, et al. 2010. Assessment of AMSR-E Antarctic winter sea-ice concentrations using Aqua MODIS. IEEE Transactions on Geoscience and Remote Sensing, 48(9): 3331–3339, doi: 10.1109/TGRS.2010.2046495
Cavalieri D J, Parkinson C L, Gloersen P, et al. 1999. Deriving long-term time series of sea ice cover from satellite passive-microwave multisensor data sets. Journal of Geophysical Research: Oceans, 104(C7): 15803–15814, doi: 10.1029/1999JC900081
Chen Haihua, Li Lele, Guan Lei. 2021. Cross-calibration of brightness temperature obtained by FY-3B/MWRI using Aqua/AMSR-E data for snow depth retrieval in the Arctic. Acta Oceanologica Sinica, 40(1): 43–53, doi: 10.1007/s13131-021-1717-2
Comiso J C. 1995. SSM/I sea ice concentrations using the bootstrap algorithm. Washington, DC: National Aeronautics and Space Administration, 40
Comiso J C, Cavalieri D J, Markus T. 2003. Sea ice concentration, ice temperature, and snow depth using AMSR-E data. IEEE Transactions on Geoscience and Remote Sensing, 41(2): 243–252, doi: 10.1109/TGRS.2002.808317
Comiso J C, Kwok R. 1996. Surface and radiative characteristics of the summer Arctic sea ice cover from multisensor satellite observations. Journal of Geophysical Research: Oceans, 101(C12): 28397–28416, doi: 10.1029/96JC02816
Comiso J C, Meier W N, Gersten R. 2017. Variability and trends in the Arctic Sea ice cover: results from different techniques. Journal of Geophysical Research: Oceans, 122(8): 6883–6900, doi: 10.1002/2017JC012768
Cvijanovic I, Caldeira K, MacMartin D G. 2015. Impacts of ocean albedo alteration on Arctic sea ice restoration and Northern Hemisphere climate. Environmental Research Letters, 10(4): 044020, doi: 10.1088/1748-9326/10/4/044020
Gloersen P, Cavalieri D J. 1986. Reduction of weather effects in the calculation of sea ice concentration from microwave radiances. Journal of Geophysical Research: Oceans, 91(C3): 3913–3919, doi: 10.1029/JC091iC03p03913
Hall D K, Key J R, Casey K A, et al. 2004. Sea ice surface temperature product from MODIS. IEEE Transactions on Geoscience and Remote Sensing, 42(5): 1076–1087, doi: 10.1109/TGRS.2004.825587
Hao Guanghua, Su Jie. 2015. A study on the dynamic tie points ASI algorithm in the Arctic Ocean. Acta Oceanologica Sinica, 34(11): 126–135, doi: 10.1007/s13131-015-0659-y
Kaleschke L, Lüpkes C, Vihma T, et al. 2001. SSM/I sea ice remote sensing for mesoscale ocean-atmosphere interaction analysis. Canadian Journal of Remote Sensing, 27(5): 526–537, doi: 10.1080/07038992.2001.10854892
Lavelle J, Tonboe R, Tian T, et al. 2016. Product user manual for the OSI SAF AMSR-2 global sea ice concentration. Product OSI-408. Copenhagen, Denmark: Danish Meteorological Institute
Li Xinqing, Cheng Xiao, Hui Fengming, et al. 2016. Analysis of sea ice conditions in the Arctic northeast passage in summer 2014. Chinese Journal of Polar Research (in Chinese), 28(1): 87–94
Liu Sen, Zou Bin, Shi Lijian, et al. 2020. Polar sea ice concentration retrieval based on FY-3C microwave radiation imager data. Haiyang Xuebao (in Chinese), 42(1): 113–122
Markus T, Cavalieri D J. 2000. An enhancement of the NASA Team sea ice algorithm. IEEE Transactions on Geoscience and Remote Sensing, 38(3): 1387–1398, doi: 10.1109/36.843033
Markus T, Cavalieri D J. 2009. The AMSR-E NT2 Sea Ice Concentration Algorithm : its Basis and Implementation. The Remote Sensing Society of Japan, 29(1): 216–225
Meier W N, Fetterer F, Stewart J S, et al. 2015. How do sea-ice concentrations from operational data compare with passive microwave estimates? Implications for improved model evaluations and forecasting. Annals of Glaciology, 56(69): 332–340, doi: 10.3189/2015AoG69A694
Parkinson C L. 1987. Arctic Sea Ice, 1973–1976: Satellite Passive-Microwave Observations. Washington, DC: Scientific and Technical Information Branch, NASA
Perovich D K, Nghiem S V, Markus T, et al. 2007. Seasonal evolution and interannual variability of the local solar energy absorbed by the Arctic Sea ice-ocean system. Journal of Geophysical Research: Oceans, 112(C3): C03005
Smith D M. 1996. Extraction of winter total sea-ice concentration in the Greenland and Barents Seas from SSM/I data. International Journal of Remote Sensing, 17(13): 2625–2646, doi: 10.1080/01431169608949096
Spreen G, Kaleschke L, Heygster G. 2008. Sea ice remote sensing using AMSR-E 89-GHz channels. Journal of Geophysical Research: Oceans, 113(C2): C02S03
Steffen K, Schweiger A. 1991. NASA team algorithm for sea ice concentration retrieval from Defense Meteorological Satellite Program special sensor microwave imager: comparison with Landsat satellite imagery. Journal of Geophysical Research: Oceans, 96(C12): 21971–21987, doi: 10.1029/91JC02334
Tang Xiaotong, Chen Haihua, Guan Lei, et al. 2020. Intercalibration of FY-3B/MWRI and GCOM-W1/AMSR-2 brightness temperature over the Arctic. Journal of Remote Sensing (Chinese), 24(8): 1032–1044
Tonboe R, Lavelle J, Pfeiffer R H, et al. 2016. Product user manual for OSI SAF global sea ice concentration. Product OSI-401-b. Copenhagen, Denmark: Danish Meteorological Institute
Wang Xiaoyu, Guan Lei, Li Lele. 2018. Comparison and validation of sea ice concentration from FY-3B/MWRI and Aqua/AMSR-E observations. Journal of Remote Sensing (in Chinese), 22(5): 723–736
Wiebe H, Heygster G, Markus T. 2009. Comparison of the ASI ice concentration algorithm with Landsat-7 ETM+ and SAR imagery. IEEE Transactions on Geoscience and Remote Sensing, 47(9): 3008–3015, doi: 10.1109/TGRS.2009.2026367
Wu Zhankai, Wang Xingdong, Wang Xuemei. 2019. An improved ARTSIST sea ice algorithm based on 19 GHz modified 91 GHz. Acta Oceanologica Sinica, 38(10): 93–99, doi: 10.1007/s13131-019-1482-7
Wu Zhankai, Wang Xingdong, Wang Feng. 2020. Study on Arctic sea ice concentration based on FY-3 MWRI data. Journal of Glaciology and Geocryology (in Chinese), 42(4): 1135–1144
Yang Hu, Zou Xiaolei, Li Xiaoqing, et al. 2012. Environmental data records from FengYun-3B microwave radiation imager. IEEE Transactions on Geoscience and Remote Sensing, 50(12): 4986–4993, doi: 10.1109/TGRS.2012.2197003
Ye Xinxin, Su Jie, Wang Yang, et al. 2011. Assessment of AMSR-E sea ice concentration in ice margin zone using MODIS data. In: 2011 International Conference on Remote Sensing, Environment and Transportation Engineering (RSETE). Nanjing, China: IEEE, 3869–3873
Zhai Zhaokun, Lu Shanlong, Wang Ping, et al. 2017. Optimization of FY arctic sea ice dataset based on NSIDC sea ice product. Journal of Geo-information Science (in Chinese), 19(2): 143–151
Zhang Shugang. 2012. Sea ice concentration algorithm and study on the physical process about sea ice and melt-pond change in central Arctic (in Chinese) [dissertation]. Qingdao: Ocean University of China
Zhang Shugang, Zhao Jinping, Frey K, et al. 2013. Dual-polarized ratio algorithm for retrieving Arctic sea ice concentration from passive microwave brightness temperature. Journal of Oceanography, 69(2): 215–227, doi: 10.1007/s10872-012-0167-z
Zhao Jinping, Ren Jingping. 2000. Study on the method to analyze parameters of Arctic sea ice from airborne digital imagery. Journal of Remote Sensing (in Chinese), 21(4): 271–278